CHEMISTRY OF MATERIALS

Article

pubs.acs.org/cm

Transparent Porous Polysaccharide Cryogels Provide Biochemically Defined, Biomimetic Matrices for Tunable 3D Cell Culture

Roger Y. Tam,[†] Stephanie A. Fisher,[†,‡] Alexander E. G. Baker,[†,‡] and Molly S. Shoichet*[,†,‡,§]

[†]Department of Chemical Engineering and Applied Chemistry, University of Toronto, 200 College Street, Toronto, Ontario, Canada M5S 3E5

[‡]Institute of Biomaterials and Biomedical Engineering, University of Toronto, 164 College Street, Toronto, Ontario, Canada M5S 3G9

[§]Department of Chemistry, University of Toronto, 80 St. George Street, Toronto, Ontario, Canada M5S 3H6

Supporting Information

ABSTRACT: Biomimetic scaffolds are desirable for 3D cell culture, yet optically transparent, macroporous, polysaccharide hydrogels have been limited. By incorporating soluble mono- and disaccharide additives during cryogelation, we synthesized biomimetic scaffolds and gained insight into the mechanism of their formation. The mono/disaccharide additives affect the size of ice crystal porogens and interact with polysaccharide polymers, altering cryogel pore size and mechanical properties. Importantly, gel transparency is maintained following removal of additives, enabling their use as biomimetic extracellular matrices. We demonstrate both optical transparency with 3D spatial control of immobilized bioactive growth factors using multiphoton patterning and cellular response to immobilized ligands.

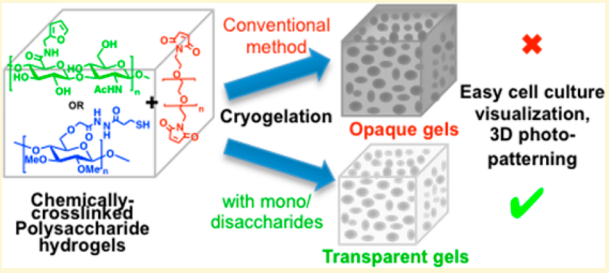

INTRODUCTION

Hydrogels have been engineered as extracellular matrix (ECM) analogues to provide chemical and physical cues to recapitulate natural cell growth.[1] Hydrogel porosity enables adequate gas and nutrient diffusion and affects cell adhesion and cell secretion of ECM molecules, with optimal cell growth often dependent on pore size.[2,3] Many strategies have been pursued to introduce pores into hydrogels.[4] Cryogelation is particularly attractive as porous hydrogels are formed by freeze/thaw methods, which are effective and facile to perform. Pore formation by ice porogens in poly(vinyl alcohol) cryogels has been described in detail,[5] and cryogels have been prepared with both natural and synthetic polymers for biomedical applications;[6,7] however, the lack of optical transparency has limited their widespread use in cell culture.[7,8] Several strategies have been used to introduce transparency into porous cryogels composed of synthetic polymers,[9−12] but reports with transparent, porous hydrogels comprising natural polymers have been limited.[11]

Polysaccharide-based polymers, such as hyaluronan, are an important class of biomaterials in tissue engineering, as they form a major component of the native ECM and are often bioactive. While polysaccharide cryogels have been reported by several groups,[6,13,14] gel transparency following the freeze/thaw process has eluded the community.

Herein, we describe, for the first time, a broadly applicable method to synthesize macroporous polysaccharide-based cryogels, with tunable pore sizes that remain transparent following freeze/thaw (Figure 1). Transparency and tunability

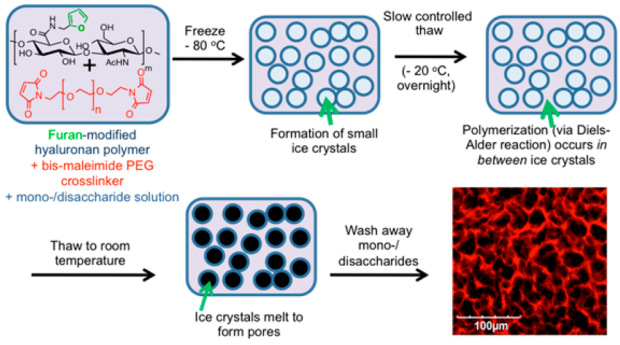

Figure 1. Schematic representation to prepare transparent, porous, chemically cross-linked HA−furan/bis-maleimide PEG hydrogels via cryogelation.

are key for 3D patterning and cell culture. We demonstrate this methodology for chemically cross-linked cryogels composed of hyaluronan (HA), which is expressed in various tissues and tumor microenvironments,[15,16] and demonstrate the broad applicability of this strategy with cross-linked methyl cellulose (MC, Figure S1), which is often used in suspension cell culture.[17]

For HA cryogels, we demonstrate the effect of using multiple simple carbohydrate additives on the optical transparency, pore

Received: February 11, 2016
Revised: April 25, 2016
Published: April 27, 2016

DOI: 10.1021/acs.chemmater.6b00627
Chem. Mater. 2016, 28, 3762−3770

size, and mechanical properties. Importantly, these gels remain transparent after the additives are removed (which differs from other polyol-based optically clearing techniques where these additives must be retained in the sample to maintain transparency[18,19]), thus enabling facile visualization of cells cultured therein and multiphoton biochemical patterning of growth factors in defined 3D volumes. Unlike previous studies where particulate sugar has been used as porogens in tissue engineered scaffolds,[20,21] here dissolved sugars interact strongly with water molecules during the freezing process and affect the structural organization of growing ice crystals and thereby ice crystal size during recrystallization.[22] Interestingly, the sugar−water interaction has been used in cellular cryopreservation,[23] protein formulation,[24] and food storage,[25] leading us to hypothesize that cryogel formulation could be manipulated by the specific sugar used.

EXPERIMENTAL SECTION

Materials. Dried sodium hyaluronate (HA) (289 kDa), was purchased from Lifecore Biomedical (Chaska, MN, U.S.A.). Bis(*N*-ethylmaleimide)−poly(ethylene glycol) (PEG-$(mal)_2$, 3 kDa) was purchased from RAPP Polymere GmbH (Tubingen, Germany). 4-(4,6-Dimethoxy-1,3,5-triazin-2-yl)-4-methyl-morpholinium chloride (DMTMM), dimethyl sulfoxide (DMSO), diisopropylcarbodiimide (DIC), borane dimethylamine complex, triisopropylsilane and maleimide−streptavidin, *N*-(2-hydroxy-ethyl)maleimide, and hyaluronidase (isolated from bovine testes, 890 U/mg) were purchased from Sigma-Aldrich (St. Louis, MO, U.S.A.). Tetrakis(triphenylphosphine) palladium was purchased from TCI America (Philadelphia, PA, U.S.A.). Amino acids for peptide synthesis were purchased from Anaspec (Fremont, CA, U.S.A.). Furfurylamine was purchased from Acros Organics (New Jersey, NJ, U.S.A.). D-Galactose, D-glucose, D-trehalose, and D-sucrose were purchased from BioRad. 2-(*N*-Morpholino)-ethanesulfonic acid (MES) and 2-[(2-hydroxy-1,1-bis-(hydroxymethyl)ethyl)amino] ethanesulfonic acid (TES) buffer were purchased from Bioshop Canada Inc. (Burlington, ON, Canada). 5-Dulbecco's phosphate-buffered saline (PBS) was purchased from Multicell Technologies Inc. (Woonsocket, RI, U.S.A.). AlexaFluor 488−hydrazide, AlexaFluor 546−maleimide, AlexaFluor 633−*N*-hydroxy succinimide (NHS), AlexaFluor 488 Phalloidin, goat antimouse AlexaFluor 633, Hoescht 33342, and 4′,6-diamidino-2-phenylindole (DAPI) were purchased from Life Technologies (Burlington, Canada). Dialysis membranes were purchased from Spectrum Laboratories Inc. (Rancho Dominguez, CA, U.S.A.). Collagen IV was purchased from Corning (Corning, NY, U.S.A.). Recombinant human epidermal growth factor (EGF) was purchased from PeproTech Inc. (Rocky Hill, NJ, U.S.A.).

General Preparation of HA−furan/PEG Cryogels. Furan-modified HA/PEG−$(maleimide)_2$ cryogels were prepared as previously described[16] with the following modifications: For 800 μL of a 1.25% HA/PEG−cryogel, HA−furan (47% substitution, 10.0 mg, 1.0 equiv of furan) was dissolved in 166 μL of 10 mM MES buffer (pH 5.5). In another vial, PEG−$(mal)_2$ (14.7 mg, 0.8 equiv of maleimide relative to furans) was dissolved in 57.9 μL of 10 mM MES buffer (pH 5.5) and then mixed with the HA−furan solution. To enhance cryogel transparency, a 1.34 M carbohydrate solution (one of D-galactose, D-glucose, D-trehalose, or D-sucrose dissolved in 10 mM MES buffer (pH 5.5)) was prepared and added to the HA/PEG solution and diluted with 10 mM MES buffer (pH 5.5) to achieve the desired sugar concentration. The gel solution was thoroughly mixed using a vortex, followed by centrifugation to remove air bubbles. The solution was then transferred into the desired vessels and incubated at 37 °C for 1 h. Gels were placed in a −80 °C freezer for 45 min, followed by storage at −20 °C overnight. The gels were removed and thawed at room temperature, and the freeze−thaw cycle (i.e, −80 °C freezer for 45 min, followed by storage at −20 °C overnight) was repeated another two times. The free mono- and disaccharides were then removed from the cryogels by extensive washing with PBS.

For cell experiments and pore size analyses, 30 μL of gel (prepared with 0.96 M galactose or sucrose) was prepared in each well in a 96 well plate. For absorbance measurements and uncompressed mechanical testing, 75 μL of gel were prepared in 96-well plates or in 16-well glass chamber slides, respectively. For hydrogel swelling and degradation studies, 100 μL of gels were prepared in pretared 1.6 mL Eppendorf tubes. For photopatterning experiments, 100 μL of each gel (prepared with 0.96 M trehalose or sucrose) was prepared in 8-well glass chamber slides.

Absorbance Measurements of HA−furan/PEG Cryogels. Cryogels were prepared in a 96 well plate, with 75 μL per well. Each gel was prepared in triplicate and measured at 370 and 740 nm on a Tecan Plate Reader. Gels were thoroughly washed with PBS prior to performing absorbance measurements. Absorbance values of the cryogels were recorded and converted to percent transmittance.

Pore Size Characterization. For pore size analysis, 30 μL of gel was prepared in each well in a 96-well plate. Following cryogel formation, the unreacted furans in the HA/PEG gel were reacted with AlexaFluor 546−maleimide to enable visualization of the pore walls. HA/PEG-cryogels were swelled in MES buffer (0.1 M, pH 5.5), and maleimide−AlexaFluor 546 (2 ng dye/μL gel) was added and mixed overnight at room temperature in the dark. The labeled gels were washed extensively with PBS to remove unbound dye. At least three gels were prepared for each formulation, and Z-stack sections of each gel were imaged using an Olympus confocal microscope at 20× magnification. Pore sizes were quantified at varying depths within a Z stack (25, 100, 200, 300 μm) using ImageJ software.

Mechanical Compression Testing. The Young's moduli were determined for HA−furan/PEG cryogels that were washed and preswollen in PBS, with diameters of 5 mm. Samples were placed between two impermeable flat platens connected to a DAQ−Nano17 force transducer (ATI Industrial Automation) on a Mach-1 micromechanical system (Biomomentum) and subjected to an initial tare force of 0.01 N to even out surface defects, with the platen-to-platen separation taken as the initial sample height. Uniaxial, unconfined compression was performed at 37 °C at a deformation rate of 10 μm/s until an applied strain of 20% was reached. The Young's modulus was taken as the slope of the resultant stress versus strain chart for each sample. At least five separate gels were prepared and analyzed for each gel formulation.

Fluorescence Measurements of HA−Furan/PEG Cryogels. Cryogels were prepared in a 96-well black with transparent-bottom plates, at 50 uL/well. Cryogel formulations were prepared using 1.0 mol equiv of maleimides relative to amount of furans conjugated to the HA backbone. Each gel was prepared in triplicate. Unreacted furans in the HA/PEG cryogels were reacted with maleimide−AlexaFluor 546 (5.0 μL of a 0.97 μM stock solution) and washed extensively with methanol (3 times), followed by PBS (4 times), until fluorescence was absent in the supernatant. An adsorption control was also performed by first incubating maleimide−AlexaFluor546 in 0.1 N NaOH for 3 h at room temperature to hydrolyze the base-sensitive maleimide groups to prevent their conjugation to HA−furans; the same molar amount of dye was added to the adsorption control wells. A standard curve was performed by adding a known volume of maleimide−AlexaFluor 546 dye to each respective cryogel formulation. Fluorescence intensity was measured by taking three images along the same Z-plane for each gel (three gels per condition) and quantified using ImageJ Software.

Hydrogel Swelling. HA/PEG hydrogels and cryogels were prepared (100 μL volume of gel) in a pretared 1.6 mL Eppendorf tube, using the method described above. The 1.25% HA−furan gels were prepared, with 0.78 M of each mono- or disaccharide. At least four replicates of each gel condition were prepared. Gels were washed and equilibrated in PBS at 37 °C for 24 h. At each desired time point, the buffer was removed and the gels in each tube were weighed using the same microbalance. Swelling data was reported as a ratio of gel mass at each specific day to the initial equilibrated hydrogel mass.

Hydrogel Degradation with Hyaluronidase. Hydrogels were prepared and equilibrated as described above for hydrogel swelling experiments. Each gel (100 μL) was treated with 100 μL of hyaluronidase (20 U in 100 μL, diluted in PBS) and incubated at 37

DOI: 10.1021/acs.chemmater.6b00627
Chem. Mater. 2016, 28, 3762−3770

°C overnight. At each time point, the hyaluronidase solution was removed and the gels in each tube were weighed using the same microbalance. A fresh solution of hyaluronidase (20 U in 100 μL diluted in PBS) was added at each time point.

Chemical Modification of Growth Factors for Cryogel Immobilization. Iodo−acetamide−EGF−AlexaFluor 488 was prepared as previously described.[16] Briefly, to a solution of recombinant EGF (1.0 mg, 6.21 kDa, 0.16 μmol in TES buffer, pH 8.6, PeproTech), four portions of sulfosuccinimidyl (4-iodoacetyl)aminobenzoate (sulfo−SIAB, 2.0 mg, 4.0 μmol per portion) was added dropwise every 2 h at room temperature. Unreacted sulfo−SIAB was removed by extensive dialysis in TES buffer at pH 8.0. Electrospray ionization mass spectrometry shows that an average of 3−6 iodoacetamide moieties were conjugated to EGF. To fluorescently label IA-EGF, carboxylic acids of IA-EGF were then reacted with DMT-MM and AlexaFluor 488−hydrazine and mixed overnight. Unbound fluorescent AF-488 was removed by extensive dialysis in PBS.

For recombinant EGF: ESI calcd $[M + H]^+$ = 6218.74; found 6215.8. For IA-EGF: ESI calcd 3 IA, $[M + H]^+$ = 7078.96; 4 IA, $[M + H]^+$ = 7365.71; 5 IA, $[M + H]^+$ = 7652.46; 6 IA, $[M + H]^+$ = 7939.21; found 7076.6, 7363.5, 7650.5, 7937.4, respectively.

Biotinylated-CNTF−AlexaFluor 633 was expressed and modified as previously described.[26] Briefly, a biotin−ligase recognition sequence and a hexahistidine sequence were incorporated into the C-terminus of the expressed protein (27.98 kDa, ε = 33, 570 M^{-1} cm^{-1}) to enable site-specific biotinylation and purification with a Ni-NTA column, respectively. Following biotinylation with a biotin ligase kit, biotinylated-CNTF was extensively dialyzed in PBS. Electrospray ionization mass spectrometry of biotin−CNTF shows a shift of +227 Da compared to unmodified CNTF, indicating conjugation of a single biotin moiety. Biotin−CNTF was then fluorescently labeled by adding AlexaFluor 633−NHS to react with the free amines of biotin−CNTF. Unbound dye was removed by extensive dialysis in PBS.

For recombinant CNTF, ESI calc for $[a_{n-1}]^+$ = 27801.01, $[b_{n-1} + H_2O]^+$ = 27847.02; found 27798.0, 27846.0. For biotin−CNTF, ESI calcd for $[a_{n-1}]^+$ = 28027.09, $[b_{n-1} + H_2O]^+$ = 28073.10, $[x_{n-1}]^+$ = 28104.09; found 28024.0, 28073.0, 28104.0.

Cryogel Preparation for Photopatterning. For photopatterning experiments, HA−furan/bromo-hydroxy coumarin (Bhc) was prepared as previously reported[16] with the following modification: following conjugation of Bhc−cysteamine to the HA−furan backbone with DMT-MM, the mixture was treated with 2 equiv of K_2CO_3 (relative to moles of conjugated furans) overnight at room temperature prior to dialysis in PBS and then distilled water. Substitution of Bhc was quantified using 500 MHz ^{1}H NMR. Following lyophilization to afford a white amorphous solid, cryogels were prepared as above. The unreacted furans on the HA backbone were quenched by adding 10 mg/mL *N*-ethylhydroxy maleimide (0.2 mL) in 0.1 M MES buffer (pH 5.5) and incubated overnight at room temperature. Gels were then washed with TES buffer (pH 8.6) to remove and hydrolyze unbound *N*-ethyl hydroxymaleimides. Gels were then incubated and washed three times with 0.1 M phosphate buffer (pH 6.8). Iodoacetamide−EGF, maleimide−AF546, or maleimide−streptavidin was then diluted in PBS (pH 6.8), and 100 μL was added to the gels and agitated for 2 h prior to photopatterning.

Confocal Settings for Photopatterning and Fluorescence Imaging. All patterns were created using a Leica TCS-SP2 confocal microscope (Leica Microsystems, Wetzlar, Germany) equipped with a multiphoton Mai Tai broadband Ti−sapphire laser (Spectra-Physics) using a 20× objective (NA = 0.4) and an electronic stage. The multiphoton laser was set to 740 nm with an offset of 75% and a gain of 35% for patterning.

Images were collected by using an inverted confocal microscope (Olympus FV1000) at 10× or 20× magnification using the following excitation and emission wavelengths: for AlexaFluor 488: Ex. 485 nm, Em. 520 nm; for AlexaFluor 546, Ex. 560 nm, Em. 580 nm; for AlexaFluor 633, Ex. 635 nm, Em. 680 nm.

Synthesis of ECM-Mimetic peptides. The cell adhesive peptides Ac-GRGDS-PASSKG_4SRL_6KK(male-imide)G and(maleimide)-GRKQAAS-IKVAV-SG_4SRL_6-KK(Alloc)G were synthesized using standard Fmoc chemistry on a CEM solid phase peptide synthesizer. The 0.1 M HOBt was added to the 20% piperidine deprotection solution to prevent aspartamide formation.[27] Fmoc-lys(Alloc)-OH was first immobilized to Fmoc-Gly-Wang resin using manual solid phase peptide synthesis and monitored using the TNBS test. For the RGD peptide with C-terminal maleimide functionalization, further modifications were performed manually following automated peptide synthesis. Following the final N-terminal Fmoc deprotection step, the peptide (0.5 mmol) was acetylated using acetic anhydride (0.25 mL, 2.65 mmol) and diisopropylethylamine (0.91 mL, 5.3 mmol) in dichloromethane (10 mL) at room temperature for 2 h. The allyloxycarbonyl (alloc) group was removed using $Pd(PPh_3)_4$ (cat.) and borane dimethylamine complex (60 mg, 1.0 mmol) in dichloromethane, under $N_2(g)$ overnight at room temperature. Maleimide propanoic acid (169 mg, 1.0 mmol) was then immobilized to the peptide using the carboxylic acid activator diisopropylcarbodiimide (DIC, 0.3 mL, 2.0 mmol) in dichloromethane overnight. Finally, the peptide was cleaved from the resin using 15 mL of the cleavage cocktail: 8:1:1 (v/v/v) of TFA:H_2O:triisopropylsilane. The peptide was purified using C_{18} reversed phase HPLC (mobile phase: 15:85 to 50:50 (v:v) acetonitrile/water gradient over 30 min) and dissolved in 10% DMSO in 0.1 M MES buffer (pH 5.5) at a final peptide concentration of 0.75 mM.

Cryogels were first equilibrated in 0.1 M MES buffer (pH 5.5), and the peptides (3.75 μL of 0.75 mM peptide solutions) were added to each gel and incubated overnight. The following day, gels were washed extensively with PBS to remove unbound peptides.

Ac-GRGDS-PASSKG_4SRL_6RRKK(maleimide)G: ESI calcd for $C_{125}H_{217}N_{43}O_{38}$ $[M + H]^+$ 2929.64; found 2929.7. (Maleimide)-GRKQAAS-IKVAV-SG_4SRL_6R_2KK(Alloc)-G: ESI calcd for $C_{146}H_{258}N_{48}O_{40}$ $[M + H]^+$ 3324.96; found 3324.9.

Peptide Immobilization to Cryogels. Peptides were grafted to the preformed cryogel via Diels−Alder reaction between the unreacted furans on the HA backbone and the maleimide of the peptides. Following cryogel preparation, the gels were washed extensively with PBS to remove excess carbohydrates and unreacted polymers. Gels were then equilibrated with 0.1 M MES buffer (pH 5.5). A total of 50 μL of desired peptide solution (56 μM in 0.1 M MES buffer pH 5.5) was then added to each well and incubated overnight at 37 °C. Peptides were washed extensively with PBS and then 0.1 M MES (pH 5.5). Maleimide−AlexaFluor 546 (50 μL of 0.5 μg/mL 0.1 M MES pH 5.5) was added to each well, reacted overnight, and then washed with PBS.

Cell Culture of Human T47D Breast Cancer Cells. T47D cells (ATCC, Manassas, U.S.A.) were cultured in RPMI-1640 medium supplemented with 10% fetal bovine serum, 1% penicillin/streptomycin, and 10 μg/mL insulin at 37 °C with 5% CO_2. Cells were passaged using 0.25% trypsin for 3 min at 37 °C and inhibited using RPMI-1640 media. A total of 2000 cells in 100 μL of media were added to each well and incubated at 37 °C with 5% CO_2. After the cells settled in the gels for 45 min, another 50 μL of media supplemented with Collagen IV (20 μg/mL) and IKVAV peptide (50 μM) was added. Media were changed every 3 d. After 7 d, cells were fixed with 4% PFA for immunocytochemistry.

Immunocytochemistry. To fix cells cultured in cryogels, media were first carefully removed using a pipet, and 50 μL of 4% PFA (dissolved in PBS) was added for 1.5 h at room temperature. Gels were then carefully washed with 200 μL of PBS (4 times, 10 min each), and 10% FBS in PBS was used to block nonspecific interactions for 1 h.

For T47D, 30 μL of AlexaFluor 488 Phalloidin (1/100 in 10% FBS) and DAPI (1/500 in 10% FBS) were added for 3 h at room temperature. Gels were then washed extensively with 1% FBS/PBS (4 times, 30 min each). Cells in the gels were imaged while still in the 96 well plates.

Statistical Analysis. All statistical analyses were performed using GraphPad Prism version 6.00 for Mac (GraphPad Software, San Diego, CA, U.S.A.). Differences among groups of three or more treatments were assessed by one-way ANOVA with Tukey or Bonferroni post hoc tests to identify statistical differences. An α

DOI: 10.1021/acs.chemmater.6b00627
Chem. Mater. 2016, 28, 3762−3770

level of 0.05 was set as the criterion for statistical significance. Graphs are annotated with p values represented as $^{*}p \leq 0.05$, $^{**}p \leq 0.01$, $^{***}p \leq 0.001$. All data are presented as mean ± standard deviation.

RESULTS AND DISCUSSION

Transparent HA cryogels are synthesized by reacting HA−furan with bismaleimide−poly(ethylene glycol) (Mal_2PEG) cross-

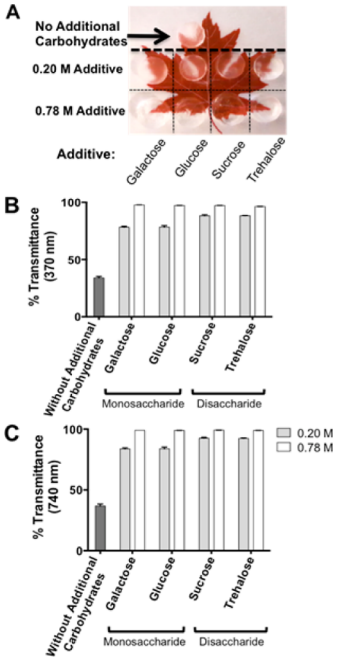

Figure 2. (A) Image of various cryogel formulations with carbohydrate additives. % transmittance of cryogels at (B) 370 nm and (C) 740 nm. Disaccharides and increased carbohydrate concentrations increased cryogel transparency.

linkers in the presence of mono- or disaccharides (Figure 1). Freezing this mixture produces ice crystals that act as porogens, with chemically cross-linked HA-PEG pore walls forming in the intergranular space between the ice crystals. We screened monosaccharides (galactose and glucose) and disaccharides (sucrose and trehalose) and hypothesized that the different physicochemical properties of these carbohydrates (e.g., hydroxyl stereochemistry, partial molar compressibility, and hydration number)[22,28] would result in HA−cryogels with different properties.

Cryogel transparency increased as carbohydrate concentrations increased (Figure 2A−C), yet cryogels formulated without additional sugars are turbid, consistent with previous examples of porous polysaccharide cryogels.[6,14] Recently, glycerol was reported to improve the transparency of macroporous PEG and gelatin chemically cross-linked hydrogels by forming intermolecular hydrogen bonds with the polymers.[11] The authors proposed that this enhanced transparency resulted in increased anisotropy of the PEG polymers, thereby reducing light scattering. However, they did not observe this clearing effect with polysaccharide gels likely because glycerol does not interact as strongly with polysaccharides as it does with PEG and gelatin. Our inclusion of simple carbohydrates may similarly improve transparency and polymer anisotropy of polysaccharide cryogels through carbohydrate−carbohydrate interactions with the HA backbone during cryogelation. Such interactions are abundant in nature

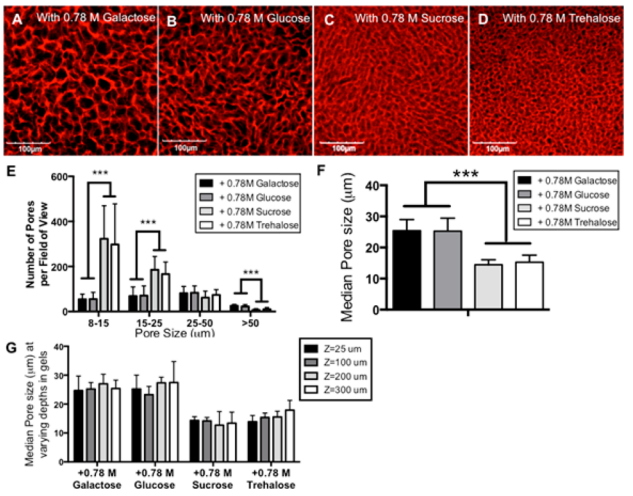

Figure 3. Carbohydrate additives alter the physical properties of HA cryogels. Representative images of cryogels prepared using monosaccharides, (A) galactose and (B) glucose, and disaccharides, (C) sucrose and (D) trehalose. (E) Pore size distribution and (F) median pore size of each gel formulation. Cryogels prepared with disaccharides had smaller pore sizes than monosaccharides. (G) Median pore size of each formulation at specific Z-axis depths within the cryogels showing no statistical differences between the Z-axis depths of each individual formulation. All data are presented as mean ± standard deviation. P values are represented as $^{***}p \leq 0.001$ one-way ANOVA Bonferonni post hoc analysis.

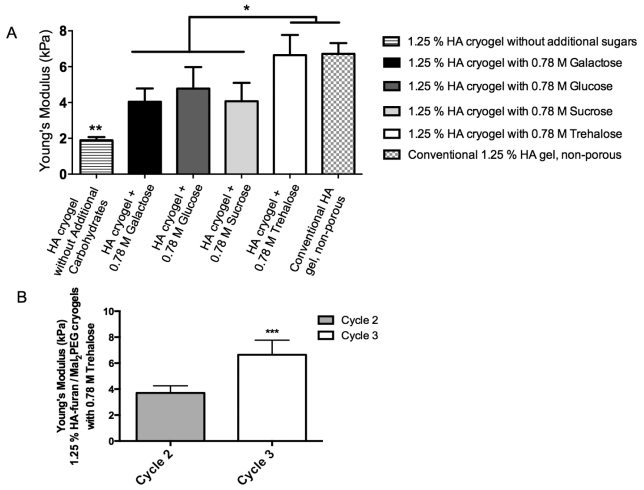

Figure 4. Bulk Young's (elastic) modulus of HA/PEG gels measured by bulk compression testing. (A) Addition of simple carbohydrates increases stiffness of cryogels that underwent three freeze−thaw cycles while addition of trehalose further increases stiffness to match that of conventional nonporous HA hydrogels ($p > 0.05$). (All data are presented as mean ± standard deviation, $n \geq 5$). P values are represented as $^{*}p \leq 0.05$, $^{**}p \leq 0.01$ one-way ANOVA Bonferroni post hoc analysis. (B) Young's modulus increases as the number of freeze/thaw cycles increases. While cryogels did not form after the first cycle, Young's modulus clearly significantly increased between cycles 2 and 3 in cryogels formulated with 0.78 M trehalose (P values are represented as $^{***}p \leq 0.001$ t test post hoc analysis, $n \geq 5$, mean ± standard deviation plotted).

and play important roles in many biological processes such as cell adhesion and recognition.[29,30]

With our interest in designing ECM-mimetic scaffolds, we sought to use these transparent cryogels for multiphoton

DOI: 10.1021/acs.chemmater.6b00627
Chem. Mater. 2016, 28, 3762−3770

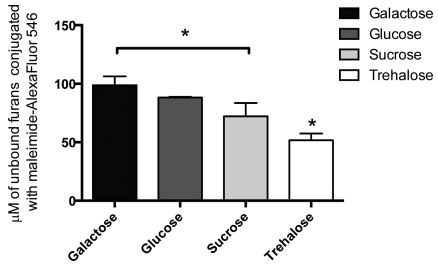

Figure 5. Unreacted furans following cryogelation in HA−furan/PEG cryogels formulated with 0.78 M mono- or disaccharides. Unreacted furans are conjugated with maleimide−AlexaFluor 546 and washed to remove unbound dye; a higher amount of fluorescence means that more furans are unreacted during cryogelation and, thus, have lower cross-linking efficiency. Significantly fewer unreacted furans were present following cryogelation with trehalose (white bar), translating to a higher degree of cross-linking efficiency. All data are presented as mean ± standard deviation. *P* values are represented as $*p \leq 0.05$, one-way ANOVA Tukey post hoc analysis, $n = 3$ gels per condition. A calibration curve with AlexaFluor 546 was generated and used for each set of cryogel formulations.

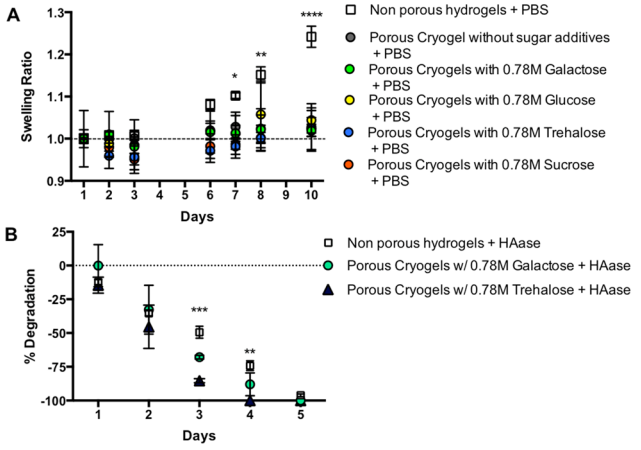

Figure 6. Stability of HA cryogels (A) swelling ratio of macroporous HA cryogels and nonporous HA gels. Gels were equilibrated in PBS for 24 h, and then the volume of the gel was measured at 37 °C in PBS relative to pre-equilibrated volume. Cryogels (circles) exhibit similar and minimal swelling, while nonporous hydrogels (square) swell by approximately 25% after 10 days. Statistics were performed for various formulations at each day using one-way ANOVA Bonferroni post hoc analysis. * = nonporous hydrogels are significantly different than all porous cryogels ($p \leq 0.05$); ** = nonporous hydrogels are significantly different than porous cryogels prepared with galactose, trehalose, and sucrose and without sugar additives ($p \leq 0.01$), *** = nonporous hydrogels are significantly different than all porous cryogels ($p \leq 0.001$) ($n = 4$, mean ± SD plotted). (B) Degradation of HA gels using hyaluronidase (20U). Porous cryogels (circle and triangle data points) degrade faster than nonporous gels (square). Statistics were performed for various formulations at each day using one-way ANOVA Bonferroni post hoc analysis. *P* values are represented as $**p \leq 0.01$ and $***p \leq 0.001$ and show statistical significance between each formulation on the same day.

confocal microscopy to immobilize bioactive molecules within a precise three-dimensional volume. Although we have previously shown that this technique can be used for conventional, nonporous transparent hydrogels,[16,31] it has not been described for cryogels due to their lack of transparency in previous formulations. Bromo-hydroxy coumarin (Bhc) is an effective photocaging group that can be cleaved using two-photon

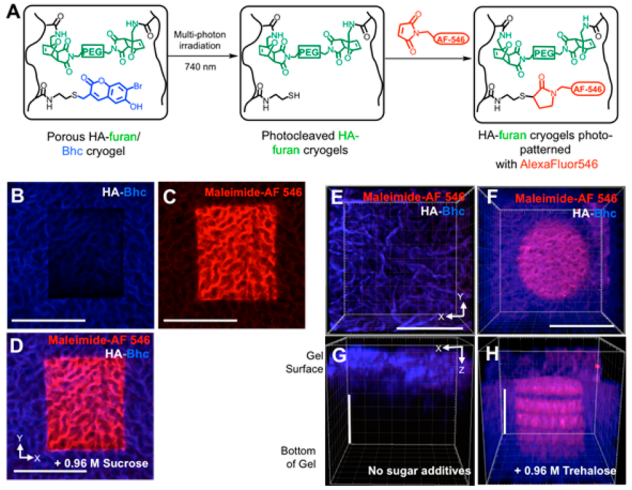

Figure 7. (A) Schematic representation of photopatterning maleimide−AlexaFluor 546 dye into HA cryogels. The photolabile group bromo-hydroxy coumarin (Bhc) can be cleaved using multiphoton confocal microscopy (740 nm) to liberate free thiols that can then react with the maleimide fluorophore. (B) Bhc immobilized to the HA−furan polymer backbone (blue fluorescence) is photolytically cleaved from HA backbone at specific regions (darkened rectangle). (C) The resulting uncaged thiols in the patterned regions are conjugated to maleimide−AlexaFluor 546 dye (red). (D) Overlay of HA-bhc pore walls (blue) and immobilized mal−AF546 dye. Unbound fluorophores are removed by extensive washing with PBS. (E, G) Photopatterning performed using turbid HA cryogels prepared in the absence of any sugar additives (E: top view, G: side view). No patterning is observed, and imaging is not possible past the surface of the gel. (F, H) Patterning performed in the presence of transparent HA cryogels showing patterning can be achieved (red circular discs) with spatial-control and observed throughout the gel (F: top view, H: side view). Scale bars represent 200 μm.

irradiation (at 740 nm), a technique that has defined *Z*-axis control.[31,32] We examined the transmittance of HA cryogels at wavelengths relevant for the photocleavage reaction (370 and 740 nm, Figure 1B,C): gels formulated in the absence of additional carbohydrates had low transmittance (~35%) whereas those formulated in the presence of increased carbohydrate concentrations had higher transmittance (78 to 93% and 96 to 99% for 0.2 and 0.78 M additional sugars, respectively). At 0.20 M, disaccharides improved the transmittance compared to monosaccharides likely because disaccharides have more hydroxyl groups and occupy greater steric volume than monosaccharides and thus have greater interactions with the HA polysaccharide, resulting in improved polymer anisotropy and thus greater optical transmittance. Interestingly, at 0.78 M, the type of carbohydrate did not affect the transmittance; the interactions between the simple sugars and polymer backbone may be saturated, resulting in a nearly transparent gel, with a cumulative average transmittance of 99.0 ± 0.1%.

To better understand how cryogel formulation influenced porosity, fluorescently labeled HA cryogels were prepared. We sought to understand the role of carbohydrates on pore sizes by examining multiple sugars. Formulations with monosaccharides (Figure 3A,B) resulted in increased pore sizes relative to those with disaccharides (Figure 3C,D). Figure 3E,F shows pore size distribution and the average pore size of these various formulations, respectively. The increased steric volume of

DOI: 10.1021/acs.chemmater.6b00627
Chem. Mater. 2016, 28, 3762−3770

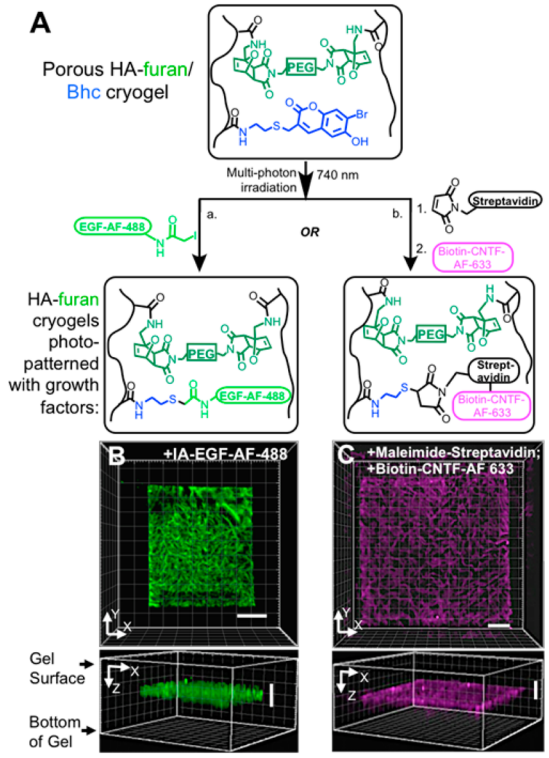

Figure 8. 3D photopatterning in porous HA cryogels immobilizes growth factors in a defined volume. (A) Synthetic scheme for protein conjugation. Confocal images of cryogels photopatterned with (B) IA−EGF−AlexaFluor 488 and (C) Mal-streptavidin and biotin−CNTF−AlexaFlor 633. Fluorescent patterns show irradiated volumes and immobilization with fluorescent biomolecules, while dark regions were not irradiated and lack protein conjugation. Scale bars represent 100 μm.

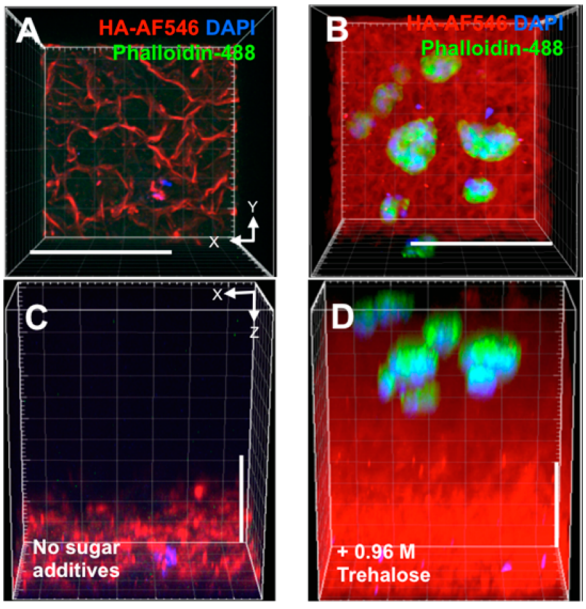

Figure 9. Imaging of T47D cells and HA cryogels using an inverted confocal microscope. Cells cultured in turbid cryogels prepared without sugar additives (A: top view; C: side view) cannot be visualized, while cells cultured in transparent cryogels with 0.96 M trehalose (B: top view, D: side view) can be readily visualized. Red = HA-AF546 pore walls; blue = DAPI; green = phalloidin−AF488. Scale bars = 200 μm.

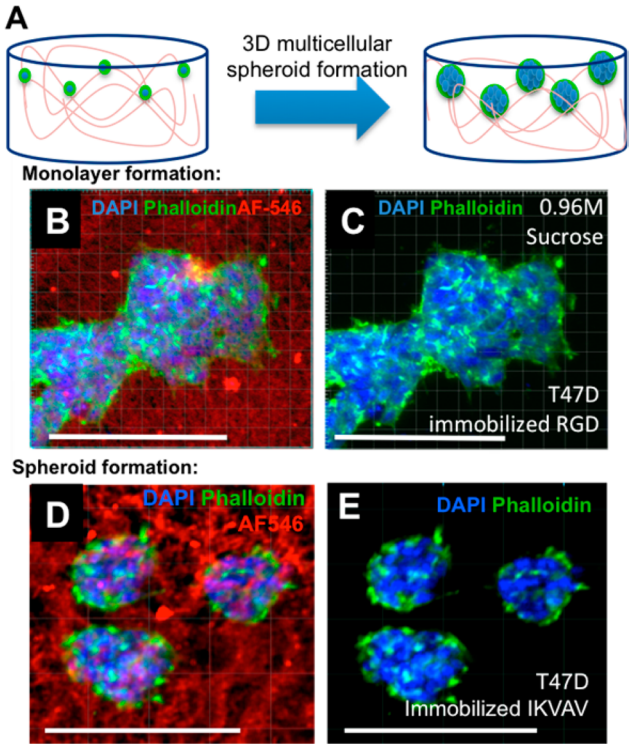

Figure 10. Cell morphology of T47D breast cancer cells cultured in HA cryogels. (A) Schematic representation of cells cultured on HA cryogels resulting in formation of 3D multicellular spheroids. Fluorescently labeled cryogels (red) immobilized with (B, C) RGD peptides result in cell monolayers whereas cryogels immobilized with (D, E) IKVAV peptides result in cellular spheroids. Scale bars represent 200 μm. blue = nuclei (DAPI); green = actin (phalloidin−AlexaFluor 488); red = HA gel pore walls (HA−furan−AlexaFluor 546).

disaccharides inhibits water addition to growing ice crystals better than monosaccharides, resulting in smaller ice crystals and subsequently smaller pores, corroborating previous reports.[23] Moreover, we examined the pore size at varying depths (from 25−300 μm) throughout the gels and show that the median pore sizes throughout these depths are not statistically different for each respective formulation, demonstrating uniformity of pore size with depth (Figure 3G).

While carbohydrates have previously been used as porogens in hydrogels,[20,21] it is important to note that our current technique is completely different. Previous reports used crystallized solid sugar particles to form pores, and inclusion of these insoluble carbohydrate porogens increased pore size.[21] However, herein we report that the soluble carbohydrate additives themselves do not act as the porogens, but rather they interact with, and decrease the size of, ice crystal porogens. Although many studies have shown that macroporous gels with pore sizes above 150−200 μm are useful for tissue regeneration applications,[3] other examples have demonstrated that smaller pore sizes are also beneficial,[4] including those used for cardiac[33] and bone[34] tissue engineering and ophthamological implants.[35] Even conventional hydrogels (with very small pore sizes) that are susceptible to enzyme degradation have been shown to support cell invasion.[36−38]

We further investigated the effect of carbohydrate additives on the Young's (elastic) modulus of the cryogels (Figure 4A) and found that addition of carbohydrates to porous cryogel formulations significantly increased the Young's modulus,

DOI: 10.1021/acs.chemmater.6b00627
Chem. Mater. 2016, 28, 3762−3770

which is consistent with a previous report.[16] Surprisingly (and not previously observed or anticipated), addition of trehalose significantly increased gel stiffness compared to other carbohydrates, resulting in a modulus that was similar to nonporous HA hydrogels ($p > 0.05$). We also show, consistent with previous reports,[14,39] that increasing the number of freeze/thaw cycles during cryogel preparation results in increased gel stiffness, Figure 4B. After one freeze/thaw cycle, gels prepared with 0.78 M trehalose did not form a gel, while increasing to two and three cycles resulted in Young's moduli of 3.7 ± 0.5 and 6.6 ± 1.1 kPa, respectively. As another control, we performed the cryogelation protocol using HA−furan only, in the absence of any maleimide−PEG cross-linker, and observed, not surpisingly, no evidence of cryogelation after three freeze/thaw cycles.

Carbohydrates increase the molecular mobility of PEG polymers in subzero conditions[40] by disrupting their incorporation into the ice lattice and suppressing the local freezing point of PEG molecules. We hypothesize that this increases the reactivity of Mal_2PEG toward HA−furan polymers under cryogenic conditions thereby increasing cross-link density and consequently stiffening the gels. Trehalose has an increased ability to disrupt the 3D hydrogen-bonded network of water molecules around ice crystals, as described by its lower partial molar compressibility value compared to other carbohydrates (-30.9×10^{-4} cm^3 mol^{-1} bar^{-1} vs that for galactose, glucose, and sucrose of −15.3, −15.9, and -17.3×10^{-4} cm^3 mol^{-1} bar^{-1}, respectively).[28] Thus, there is increased solute entropy in the intergranular space between ice crystals in trehalose formulations, resulting in increased cross-linking efficiency (and a higher modulus). We confirmed that of the mono- and disaccharide-containing formulations, trehalose has the highest degree of cross-linking (Figure 5).

Interestingly, while there is a difference in the cross-linking efficiency of these various cryogel formulations, there was no significant difference in their overall stability upon swelling at 37 °C in PBS for 1 week (Figure 6A). As a comparison, conventional, nonporous HA gels swelled by ∼25% after 10 days. Thus, while trehalose retains a similar Young's modulus compared to conventional nonporous HA gels, these cryogels are significantly more stable.

Next, we performed degradation studies of these gels using hyaluronidase, an enzyme that degrades hyaluronic acid, Figure 6B. Cryogels prepared with carbohydrates (circle and triangle data points) degraded faster than conventional, nonporous cryogels (square data points); we hypothesize this to be due to the macroporous nature of the cryogels, which enable diffusion of the enzymes throughout the gel to achieve faster bulk degradation of the cryogels.

To demonstrate the utility of this transparent scaffold, we performed 3D photopatterning of bioactive molecules using two-photon confocal microscopy, which has not been previously achieved with macroporous polysaccharide cryogels due to their lack of transparency. HA polymers were prepared for photopatterning by further modifying HA−furan to install the photoactive bromo-hydroxycoumarin (Bhc) moiety. ^{1}H NMR was used to detect the presence of Bhc (Figure S2).

Following cryogelation of Bhc-modified HA−furan cryogels, photocleavage of Bhc liberates reactive free thiols that can react with functional groups such as iodoacetamide (IA) or maleimide (Figures 7A and 8A). To prevent maleimide groups from reacting with free furans still present in the HA cryogels, we first quenched the cryogels with *N*-hydroxyethyl maleimide and then washed the gels to remove residual reagents, prior to performing the photopatterning experiments. We demonstrate that photopatterning can be achieved within transparent macroporous gels. By using confocal microscopy, we show that Bhc (which emits blue fluorescence upon excitation) is photolytically cleaved from a specific region within the gel (darkened rectangle in Figure 7B), while unpatterned regions remain blue due to the presence of uncleaved Bhc. The free thiols that are liberated following the photocleavage reaction are then reacted with a maleimide−AlexaFluor 546 fluorophore (Figure 7C, red rectangle). The presence of the immobilized fluorophore overlaps with the darkened photopatterned regions of the gel, confirming that photocleavage and subsequent fluorophore conjugation has occurred, Figure 7D.

As a control, photopatterning experiments were performed using turbid cryogels prepared in the absence of any sugar additives (Figure 7E,G), which did not result in any patterning. Moreover, we were unable to visualize Bhc-containing pore walls past approximately 150 μm into the gels. In contrast, patterning was successful at multiple depths and with spatial control using transparent macroporous cryogels, and the patterned regions were easily visible throughout the gel (Figure 7F,H).

Next, we demonstrate that this system can be applied to conjugate bioactive molecules that are modified with different reactive linkers (Figures S3 and S4, Figure 8A). As a proof of concept, we used epidermal growth factor (EGF) modified with iodoacetamide (Figure S3) and biotinylated ciliary neurotrophic growth factor (CNTF, Figure S4). Following cryogelation of Bhc-modified HA cryogels, photocleavage of Bhc liberates free thiols that react with either iodoacetamide (IA)-modified epidermal growth factor (IA−EGF−AlexaFluor 488, Figure 8B, green) or Mal−streptavidin and sequential conjugation with biotin−ciliary neurotrophic factor (biotin−CNTF−AlexaFluor 633, Figure 8C, magenta) to create fluorescent 3D rectangular patterns. The lack of fluorescence surrounding the patterns indicates that growth factor immobilization is precisely controlled along the *X*, *Y*, and *Z*-axes in porous HA cryogels.

To gain some insight into the potential use of these HA-based cryogels in cell culture, we examined cell viability and response to immobilized ligands. As the cryogels are transparent, cells were easily visualized using a standard inverted confocal microscope, which is normally difficult to achieve with conventional translucent or opaque cryogels, Figure 9. We demonstrate that these transparent gels can be imaged to greater depths (of 500 μm) than cryogels prepared in the absence of additional carbohydrates. For the latter, the depth of imaging is limited to approximately 150 μm, as was also shown in Figure 7E,G.

We performed a control experiment to demonstrate the improved imaging capabilities of our transparent cryogels. It is important to note that these gels were prepared and imaged in a 96 well plate using an inverted confocal microscope; the gels did not need to be removed from the wells to be imaged, thereby enabling live cell studies.

As proof of concept studies, we probed the formation of 3D multicellular spheroid structures with breast epithelial cells. The formation of these 3D structures is important for in vitro cancer cell culture because the majority of breast cancers originate from epithelial cells (known as carcinomas), which typically form 3D spheroid structures in lobules and ducts.[41] Finding a defined scaffold structure in which to mimic this morphology in

DOI: 10.1021/acs.chemmater.6b00627
Chem. Mater. 2016, 28, 3762−3770

vitro is limited and has led to a gap between in vitro and in vivo drug screening.[42] To this end, we envisioned using our macroporous cryogels as a platform to enable the formation of 3D multicellular spheroid structures, Figure 10A.

When T47D cells, a luminal epithelial breast cancer cell line known to form 3D spheroids,[43] were cultured on HA cryogels immobilized with the fibronectin mimetic peptide RGD, cells spread out and adhered to the cryogels (Figure 10B,C) as is typically observed in conventional 2D cell culture. In contrast, substituting RGD with a laminin 1-mimetic peptide (IKVAV, Figure S4) results in the desired 3D cell spheroid structures (Figure 10D,E), similar to what is observed in vivo. Importantly, this demonstrates that immobilization of appropriate biomimetic ligands to HA cryogels can be successfully implemented to control cellular response.

The addition (and subsequent removal) of simple carbohydrates into chemically cross-linked HA cryogel formulations increases gel transparency and alters pore size and mechanical properties. The precise control of the 3D hydrogel morphology and biomolecule immobilization enables precise control of the cellular microenvironment and consequent cellular response. Optical transparency of 3D hydrogels is critical to their utility in tissue engineering applications where in vitro cell culture and multiphoton confocal laser biomolecule patterning are enabled.

■ ASSOCIATED CONTENT

Supporting Information

The Supporting Information is available free of charge on the ACS Publications website at DOI: 10.1021/acs.chemmater.6b00627.

^{1}H NMR spectra, mass spectrometry data, and images of methyl cellulose cryogels (PDF)

■ AUTHOR INFORMATION

Corresponding Author

*(M.S.S.) E-mail: molly.shoichet@utoronto.ca.

Notes

The authors declare no competing financial interest.

■ ACKNOWLEDGMENTS

We are grateful for financial support from the Natural Sciences & Engineering Research Council of Canada (NSERC) Discovery Grant (M.S.S.), Canadian Institutes of Health Research (CIHR) Foundation grant (M.S.S.), NSERC Postgraduate Scholarship (S.A.F.), and NSERC Alexander Graham Bell Canada Graduate Scholarship (A.E.G.B.). We acknowledge the Canadian Foundation for Innovation and the Ontario Research Fund for funding of the Centre for Spectroscopic Investigation of Complex Organic Molecules and Polymers.

■ REFERENCES

(1) Engler, A. J.; Sen, S.; Sweeney, H. L.; Discher, D. E. Matrix elasticity directs stem cell lineage specification. *Cell* **2006**, *126*, 677−689.

(2) Wake, M. C.; Patrick, C. W., Jr.; Mikos, A. G. Pore morphology effects on the fibrovascular tissue growth in porous polymer substrates. *Cell Transplant.* **1994**, *3*, 339−343.

(3) Loh, Q. L.; Choong, C. Three-dimensional scaffolds for tissue engineering applications: role of porosity and pore size. *Tissue Eng., Part B* **2013**, *19*, 485−502.

(4) Annabi, N.; Nichol, J. W.; Zhong, X.; Ji, C.; Koshy, S.; Khademhosseini, A.; Dehghani, F. Controlling the porosity and microarchitecture of hydrogels for tissue engineering. *Tissue Eng., Part B* **2010**, *16*, 371−383.

(5) Ricciardi, R.; Auriemma, F.; De Rosa, C. Structure and Properties of Poly(vinyl alcohol) Hydrogels Obtained by Freeze/Thaw Techniques. *Macromol. Symp.* **2005**, *222*, 49−63.

(6) Bencherif, S. A.; Sands, R. W.; Bhatta, D.; Arany, P.; Verbeke, C. S.; Edwards, D. A.; Mooney, D. J. Injectable preformed scaffolds with shape-memory properties. *Proc. Natl. Acad. Sci. U. S. A.* **2012**, *109*, 19590−19595.

(7) Inci, I.; Kirsebom, H.; Galaev, I. Y.; Mattiasson, B.; Piskin, E. Gelatin cryogels crosslinked with oxidized dextran and containing freshly formed hydroxyapatite as potential bone tissue-engineering scaffolds. *J. Tissue Eng. Regener. Med.* **2013**, *7*, 584−588.

(8) Appel, A. A.; Anastasio, M. A.; Larson, J. C.; Brey, E. M. Imaging challenges in biomaterials and tissue engineering. *Biomaterials* **2013**, *34*, 6615−6630.

(9) Patachia, S.; Florea, C.; Friedrich, C.; Thomann, Y. Tailoring of poly(vinyl alcohol) cryogels properties by salts addition. *eXPRESS Polym. Lett.* **2009**, *3*, 320−331.

(10) Cha, W.-I.; Hyon, S.-H.; Ikada, Y. Transparent poly(vinyl alcohol) hydrogel with high water content and high strength. *Makromol. Chem.* **1992**, *193*, 1913−1925.

(11) Zhao, S.; Shen, Z.; Wang, J.; Li, X.; Zeng, Y.; Wang, B.; He, Y.; Du, Y. Glycerol-mediated nanostructure modification leading to improved transparency of porous polymeric scaffolds for high performance 3D cell imaging. *Biomacromolecules* **2014**, *15*, 2521−2531.

(12) Dalton, P. D.; Hostert, C.; Albrecht, K.; Moeller, M.; Groll, J. Structure and properties of urea-crosslinked star poly[(ethylene oxide)-ran-(propylene oxide)] hydrogels. *Macromol. Biosci.* **2008**, *8*, 923−931.

(13) Reichelt, S.; Becher, J.; Weisser, J.; Prager, A.; Decker, U.; Möller, S.; Berg, A.; Schnabelrauch, M. Biocompatible polysaccharide-based cryogels. *Mater. Sci. Eng., C* **2014**, *35*, 164−170.

(14) Plieva, F. M.; Galaev, I. Y.; Mattiasson, B. Macroporous polysaccharide cryogels. In *Macroporous Polymers*; Mattiasson, B., Kumar, A., Galaev, I. Y., Eds.; CRC Press: New York, 2010; pp 140−153.

(15) Toole, B. P. Hyaluronan: from extracellular glue to pericellular cue. *Nat. Rev. Cancer* **2004**, *4*, 528−539.

(16) Owen, S. C.; Fisher, S. A.; Tam, R. Y.; Nimmo, C. M.; Shoichet, M. S. Hyaluronic Acid Click Hydrogels Emulate the Extracellular Matrix. *Langmuir* **2013**, *29*, 7393−7400.

(17) Nasatto, P. L.; Pignon, F.; Silveira, J. L. M.; Duarte, M. E. R.; Noseda, M. D.; Rinaudo, M. Methylcellulose, a Cellulose Derivative with Original Physical Properties and Extended Applications. *Polymers* **2015**, *7*, 777−803.

(18) Ke, M. T.; Fujimoto, S.; Imai, T. SeeDB: a simple and morphology-preserving optical clearing agent for neuronal circuit reconstruction. *Nat. Neurosci.* **2013**, *16*, 1154−1161.

(19) Tsai, P. S.; Kaufhold, J. P.; Blinder, P.; Friedman, B.; Drew, P. J.; Karten, H. J.; Lyden, P. D.; Kleinfeld, D. Correlations of neuronal and microvascular densities in murine cortex revealed by direct counting and colocalization of nuclei and vessels. *J. Neurosci.* **2009**, *29*, 14553−14570.

(20) Wei, G.; Ma, P. X. Partially nanofibrous architecture of 3D tissue engineering scaffolds. *Biomaterials* **2009**, *30*, 6426−6434.

(21) Li, H.; Wijekoon, A.; Leipzig, N. D. 3D differentiation of neural stem cells in macroporous photopolymerizable hydrogel scaffolds. *PLoS One* **2012**, *7*, e48824.

(22) Tam, R. Y.; Ferreira, S. S.; Czechura, P.; Chaytor, J. L.; Ben, R. N. Hydration Index-A Better Parameter for Explaining Small Molecule Hydration in Inhibition of Ice Recrystallization. *J. Am. Chem. Soc.* **2008**, *130*, 17494−17501.

(23) Chaytor, J. L.; Tokarew, J. M.; Wu, L. K.; Leclere, M.; Tam, R. Y.; Capicciotti, C. J.; Guolla, L.; von Moos, E.; Findlay, C. S.; Allan, D. S.; Ben, R. N. Inhibiting ice recrystallization and optimization of cell viability after cryopreservation. *Glycobiology* **2012**, *22*, 123−133.

DOI: 10.1021/acs.chemmater.6b00627
Chem. Mater. 2016, 28, 3762−3770

(24) Newman, Y. M.; Ring, S. G.; Colaco, C. The role of trehalose and other carbohydrates in biopreservation. *Biotechnol. Genet. Eng. Rev.* **1993**, *11*, 263−294.
(25) Petzold, G.; Aguilera, J. M. Ice Morphology: Fundamentals and Technological Applications in Foods. *Food Biophysics* **2009**, *4*, 378−396.
(26) Wylie, R. G.; Ahsan, S.; Aizawa, Y.; Maxwell, K. L.; Morshead, C. M.; Shoichet, M. S. Spatially controlled simultaneous patterning of multiple growth factors in three-dimensional hydrogels. *Nat. Mater.* **2011**, *10*, 799−806.
(27) Vanier, G., Microwave-Assisted Peptide Synthesis (CEM). In *Peptide Synthesis and Applications*; Jensen, K. J., Shelton, P. T., Pedersen, S. L., Eds.; Humana Press: New York, 2013; pp 235−249.
(28) Galema, S.; Hoiland, H. Stereochemical aspects of hydration of carbohydrates in aqueous solutions. 3. Density and ultrasound measurements. *J. Phys. Chem.* **1991**, *95*, 5321−5326.
(29) Bucior, I.; Burger, M. M. Carbohydrate-carbohydrate interaction as a major force initiating cell-cell recognition. *Glycoconjugate J.* **2004**, *21*, 111−123.
(30) Bucior, I.; Scheuring, S.; Engel, A.; Burger, M. M. Carbohydrate-carbohydrate interaction provides adhesion force and specificity for cellular recognition. *J. Cell Biol.* **2004**, *165*, 529−537.
(31) Wylie, R. G.; Shoichet, M. S. Three-Dimensional Spatial Patterning of Proteins in Hydrogels. *Biomacromolecules* **2011**, *12*, 3789−3796.
(32) Furuta, T.; Wang, S. S.; Dantzker, J. L.; Dore, T. M.; Bybee, W. J.; Callaway, E. M.; Denk, W.; Tsien, R. Y. Brominated 7-hydroxycoumarin-4-ylmethyls: photolabile protecting groups with biologically useful cross-sections for two photon photolysis. *Proc. Natl. Acad. Sci. U. S. A.* **1999**, *96*, 1193−1200.
(33) Galperin, A.; Oldinski, R. A.; Florczyk, S. J.; Bryers, J. D.; Zhang, M.; Ratner, B. D. Integrated bi-layered scaffold for osteochondral tissue engineering. *Adv. Healthcare Mater.* **2013**, *2*, 872−883.
(34) Whang, K.; Healy, K. E.; Elenz, D. R.; Nam, E. K.; Tsai, D. C.; Thomas, C. H.; Nuber, G. W.; Glorieux, F. H.; Travers, R.; Sprague, S. M. Engineering bone regeneration with bioabsorbable scaffolds with novel microarchitecture. *Tissue Eng.* **1999**, *5*, 35−51.
(35) Teng, W.; Long, T. J.; Zhang, Q.; Yao, K.; Shen, T. T.; Ratner, B. D. A tough, precision-porous hydrogel scaffold: ophthalmologic applications. *Biomaterials* **2014**, *35*, 8916−8926.
(36) Fisher, S. A.; Anandakumaran, P. N.; Owen, S. C.; Shoichet, M. S. Tuning the Microenvironment: Click-Crosslinked Hyaluronic Acid-Based Hydrogels Provide a Platform for Studying Breast Cancer Cell Invasion. *Adv. Funct. Mater.* **2015**, *25*, 7163−7172.
(37) Lutolf, M. P.; Lauer-Fields, J. L.; Schmoekel, H. G.; Metters, A. T.; Weber, F. E.; Fields, G. B.; Hubbell, J. A. Synthetic matrix metalloproteinase-sensitive hydrogels for the conduction of tissue regeneration: engineering cell-invasion characteristics. *Proc. Natl. Acad. Sci. U. S. A.* **2003**, *100*, 5413−5418.
(38) Raeber, G. P.; Lutolf, M. P.; Hubbell, J. A. Molecularly engineered PEG hydrogels: a novel model system for proteolytically mediated cell migration. *Biophys. J.* **2005**, *89*, 1374−1388.
(39) Mao, C.-F.; Chen, J.-C. Interchain association of locust bean gum in sucrose solutions: An interpretation based on thixotropic behavior. *Food Hydrocolloids* **2006**, *20*, 730−739.
(40) Izutsu, K.; Yoshioka, S.; Kojima, S.; Randolph, T. W.; Carpenter, J. F. Effects of sugars and polymers on crystallization of poly(ethylene glycol) in frozen solutions: phase separation between incompatible polymers. *Pharm. Res.* **1996**, *13*, 1393−1400.
(41) Hirschhaeuser, F.; Menne, H.; Dittfeld, C.; West, J.; Mueller-Klieser, W.; Kunz-Schughart, L. A. Multicellular tumor spheroids: an underestimated tool is catching up again. *J. Biotechnol.* **2010**, *148*, 3−15.
(42) Hongisto, V.; Jernstrom, S.; Fey, V.; Mpindi, J. P.; Kleivi Sahlberg, K.; Kallioniemi, O.; Perala, M. High-throughput 3D screening reveals differences in drug sensitivities between culture models of JIMT1 breast cancer cells. *PLoS One* **2013**, *8*, e77232.
(43) Lagadec, C.; Vlashi, E.; Della Donna, L.; Meng, Y.; Dekmezian, C.; Kim, K.; Pajonk, F. Survival and self-renewing capacity of breast cancer initiating cells during fractionated radiation treatment. *Breast Cancer Res.* **2010**, *12*, R13.

DOI: 10.1021/acs.chemmater.6b00627
Chem. Mater. 2016, 28, 3762−3770